Supplementary material for "Density and inertia effects on two-dimensional active semiflexible filament suspensions"

Giulia Janzen[1,*] and D.A. Matoz-Fernandez[1,†]

[1] *Department of Theoretical Physics, Complutense University of Madrid, 28040 Madrid, Spain*

MODEL

Bonded interactions $\phi_B = \phi_{bond} + \phi_{bend}$ account for both chain stretching, modeled by the Tether bond potential [1] which has an attractive part ϕ_{ba}

$$\phi_{ba}(r_{ij}) = \begin{cases} \frac{k_b \exp[1/(l_{c_0} - r_{ij})]}{l_{\max} - r_{ij}} & r_{ij} > l_{c_0} \\ 0 & r_{ij} \leq l_{c_0}, \end{cases} \tag{S1}$$

and a repulsive part ϕ_{br} at short distances

$$\phi_{br}(r_{ij}) = \begin{cases} \frac{k_b \exp[1/(r_{ij} - l_{c_1})]}{r_{ij} - l_{\min}} & r_{ij} < l_{c_1} \\ 0 & r_{ij} \geq l_{c_1}, \end{cases} \tag{S2}$$

where r_{ij} represents the distance between two interacting particles, k_b is the bond stiffness, l_{c0} is the cutoff length of the attractive part of the potential, l_{max} is the maximum bond length, l_{min} is the minimum bond length, l_{c1} is the cutoff length of the repulsive part of the potentials. The parameters are set to: $k_b = 10$, $l_{max} = 1.55b$, $l_{min} = 0.2b$, $l_{c0} = 0.75b$, and $l_{c1} = 0.1b$, where $b = 0.86\sigma$. Note that in the limit of small bond-length variations which is the one that we consider here the use of Tether or FENE bond potential should not influence the results. As shown in Figure S1, the fluctuations in the polymer's length are on the order of 10^{-6}, similar to what is expected for the FENE potential.

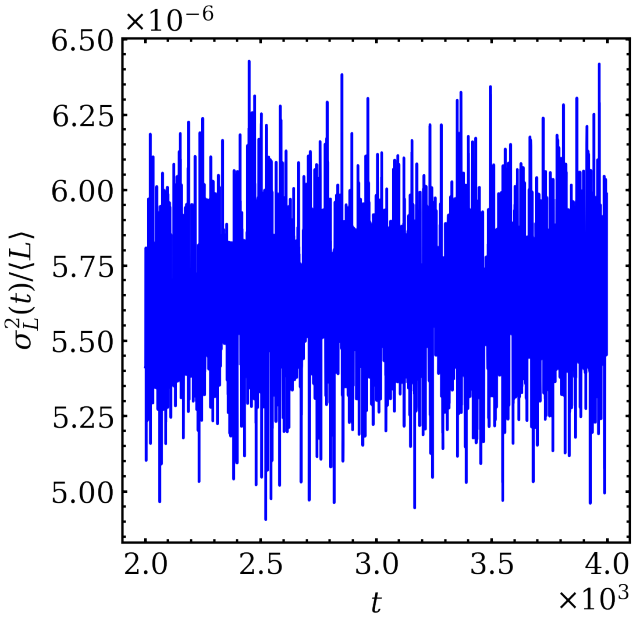

FIG. S1. Fluctuations of the polymer's length for $\rho = 0.4$, and $Pe = 10^2$. The variance of the length of the polymers σ_L^2 is normalized by the averaged length of the polymer as a function of time.

* gjanzen@ucm.es
† dmatoz@ucm.es

Next, bending is modelled with the harmonic angle potential [2]

$$\phi_{bend} = \frac{\kappa}{2}(\theta - \theta_0)^2, \tag{S3}$$

where κ is the bending stiffness, θ is the angle between the neighbouring bonds and θ_0 ($= \pi$) represents the equilibrium rest angle. The nonbonded interactions, ϕ_{NB} account for steric repulsion and are modeled with the Weeks-Chandler-Anderson (WCA) potential [3],

$$\phi_{NB}(r_{ij}) = \begin{cases} 4\epsilon \left[\left(\frac{\sigma}{r_{ij}}\right)^{12} - \left(\frac{\sigma}{r_{ij}}\right)^{6} + \Delta\phi_{pair}(r_{ij}) \right] & r_{ij} < r_{cut} \\ 0 & r_{ij} > r_{cut}, \end{cases} \tag{S4}$$

where r_{ij} represents the distance between two interacting particles, ϵ is the depth of the potential well, σ denotes the characteristic distance of the interaction, $r_{cut} = \sigma\, 2^{\frac{1}{6}}$ is the cutoff distance of the potential and the potential is shifted by $\Delta\phi_{pair}(r_{ij})$ which ensures that the potential and its derivatives smoothly go to zero.

In our simulations, default mass and stiffness values were set at $m = 1$ and $\xi_p/L = 3 \times 10^{-1}$, respectively, with periodic boundary conditions applied in all directions. We maintained $6 \times 10^{-3} \leq dt \leq 10^{-4}$, employing a larger dt for $Pe \leq 10^3$, and a smaller dt for $Pe > 10^3$. Moreover, the system was allowed to relax over $2 \times 10^4\tau$ timesteps for small Péclet numbers ($Pe \leq 10^3$) and $8 \times 10^4\tau$ timesteps for larger Péclet numbers before collecting data over $5 \times 10^4\tau$ timesteps, with $\tau = dt^{-1}$. To verify whether the system is in the steady-state configuration, we assess a dynamical property, specifically the mean-squared-displacement, across distinct time origins, and subsequently compare the outcomes. The system is in the steady state when these curves are identical. Finally, all averaged properties are computed across all filaments and 100 independent configurations.

COLLECTIVE STATIC BEHAVIOR

In addition to the structural property presented in the main text, we compute the bond-bond correlation function [4], which is defined by

$$\langle cos(\theta_s) \rangle = \left\langle \frac{\mathbf{b}_k \cdot \mathbf{b}_{k+s}}{|b_k||b_{k+s}|} \right\rangle, \tag{S5}$$

where the k-th bond is defined as $\mathbf{b}_k = \mathbf{r}_{k+1} - \mathbf{r}_k$, and $\langle . \rangle$ is the ensemble average taken over all bond vectors separated by a contour-wise separation between bonds $s < N_b$. Figure S2 shows the bond-bond correlation function for different Pe. While this correlation function should exhibit exponential decay, at high Péclet numbers, $\langle \cos(\theta_s) \rangle$ displays oscillations due to the spiral shape of the filament.

CHARACTERIZING THE POLYMER'S SHAPE

Figures S3 and S4 represent the probability distribution of the turning number at densities $\rho = 0.2$ and $\rho = 0.5$, respectively. As detailed in the manuscript, at low density (Fig.S3), once the system enters the pure spiral phase, it remains within it, with the reentrant phase being absent. Conversely, at high density (Fig.S4), under high Pe, the system never exhibits a pure spiral phase; instead, a coexistence of spirals and open chains is observed (Fig. S4(d),(e)).

To understand why loops nest around spirals when $10^3 < Pe < 10^4$, we compared the probability distribution of the turning number ψ at $Pe = 5 \times 10^3$ corresponding to the loops. Figure S5 shows that the probability of finding these loops is higher at intermediate densities. As density increases further, the probability of finding loops decreases. This phenomenon is density-dependent: in a dilute system, there is sufficient space for all filaments to transition into spirals immediately. At intermediate densities, higher activity is required for all filaments to achieve a spiral configuration. At high densities, spirals and loops become less probable due to excluded volume effects.

Moreover, in Fig. S6, we show the end-to-end distance for passive filaments ($Pe = 0$) at low, intermediate, and high densities. For passive filaments, the end-to-end distance is approximately one at low and intermediate densities, but it slightly decreases at high density ($\rho = 0.5$). This decrease is attributed to excluded volume effects. Across all densities considered, the filaments do not exhibit a spiral shape.

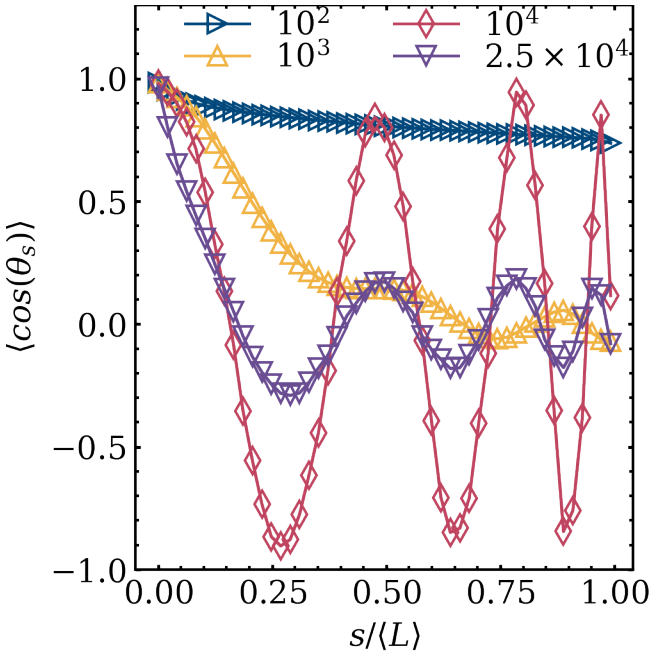

FIG. S2. Bond-bond correlation function $\langle cos(\theta_s) \rangle$ as a function of the distance $s/\langle L \rangle$ at density $\rho = 0.4$. Different colors and symbols correspond to different Peclet numbers: right blue triangles for $Pe = 10^2$, yellow triangles for $Pe = 10^3$, red diamonds for $Pe = 10^4$, and upside-down purple triangles for $Pe = 2.5 \times 10^4$.

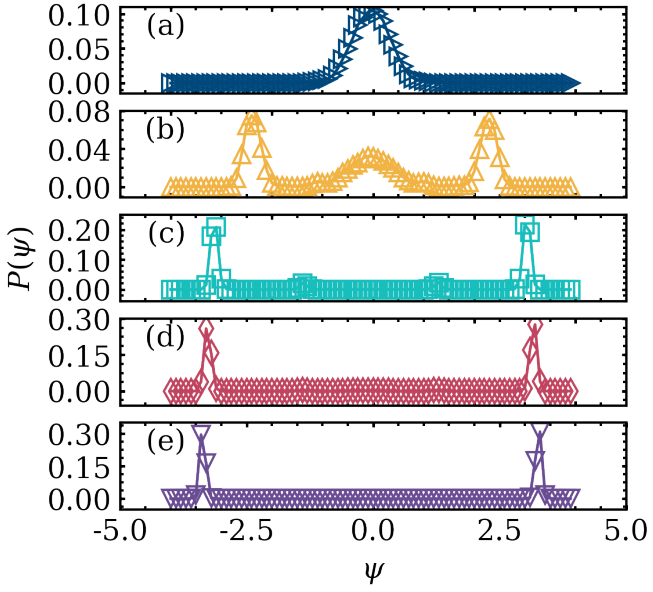

FIG. S3. Probability distribution of the turning number $P(\psi)$ at density $\rho = 0.2$. (a) The right blue triangles represent $P(\psi)$ for $Pe = 10^2$. (b) The yellow triangles correspond to $Pe = 10^3$ (c) Cyan squares represent $Pe = 5.0 \times 10^3$. (d) Red diamonds correspond to $Pe = 10^4$. (e) Upside-down purple triangles correspond to $Pe = 2.5 \times 10^4$.

ORIENTATIONAL ORDER

We compute the nematic local order parameter of the filament tangent vector $\mathbf{t}_i = (\mathbf{r}_i - \mathbf{r}_{i-1})/|\mathbf{r}_i - \mathbf{r}_{i-1}|$ at $\rho = 0.4$. The nematic order parameter is defined as:

$$S_m = \langle \cos(m\theta_{ij}) \rangle, \tag{S6}$$

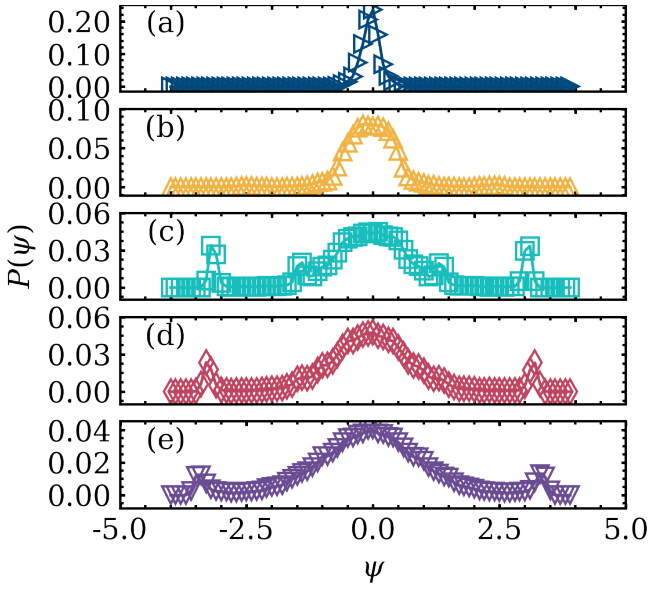

FIG. S4. Probability distribution of the turning number $P(\psi)$ at density $\rho = 0.5$. (a) The right blue triangles represent $P(\psi)$ for $Pe = 10^2$. (b) The yellow triangles correspond to $Pe = 10^3$ (c) Cyan squares represent $Pe = 5.0 \times 10^3$. (d) Red diamonds correspond to $Pe = 10^4$. (e) Upside-down purple triangles correspond to $Pe = 2.5 \times 10^4$.

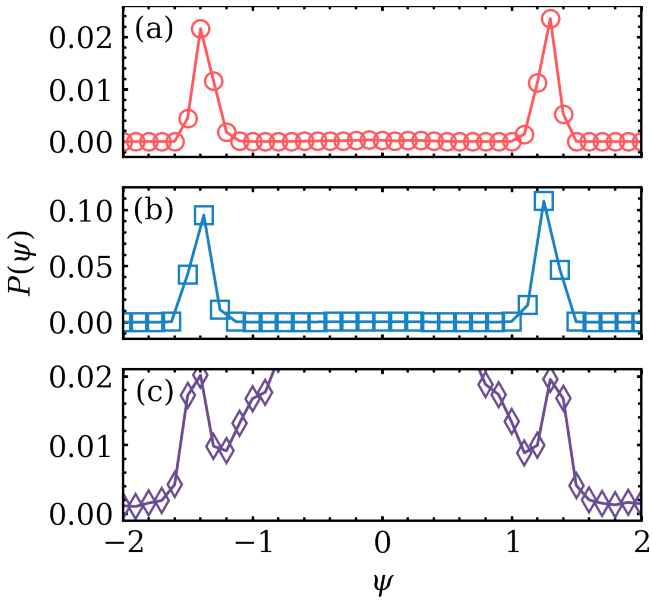

FIG. S5. Probability distribution of the turning number $P(\psi)$ at $Pe = 5 \times 10^3$ for densities: (a) $\rho = 0.2$, (b) $\rho = 0.4$, and (c) $\rho = 0.5$.

where the angle θ_{ij} between tangent vectors $\mathbf{t}_i$ and $\mathbf{t}_j$ is determined for pairs within the same or different filaments, $m = 2$ is chosen to probe the nematic order, $\langle . \rangle$ is the average over all pairs within a cutoff distance $r_c = 5\sigma$. Figure S8 shows that at low Péclet numbers, the system exhibits local nematic order similar to that observed in high-density active filaments [2] and passive polymer melts [5].

To further examine the extent of local order, we compute the spatial pair correlation function of the nematic order parameter for tangent vectors $\mathbf{t}_i$ and $\mathbf{t}_j$ separated by a distance r:

$$g_2(r) = \frac{\langle \sum_{i,j} \delta(r - |\mathbf{r}_i - \mathbf{r}_j|) \cos(2\theta_{ij}) \rangle}{\langle \sum_{i,j} \delta(r - |\mathbf{r}_i - \mathbf{r}_j|) \rangle}. \tag{S7}$$

Figure **??** shows that at low Péclet numbers, when the system exhibits nematic order, $g_2(r)$ decays consistently with

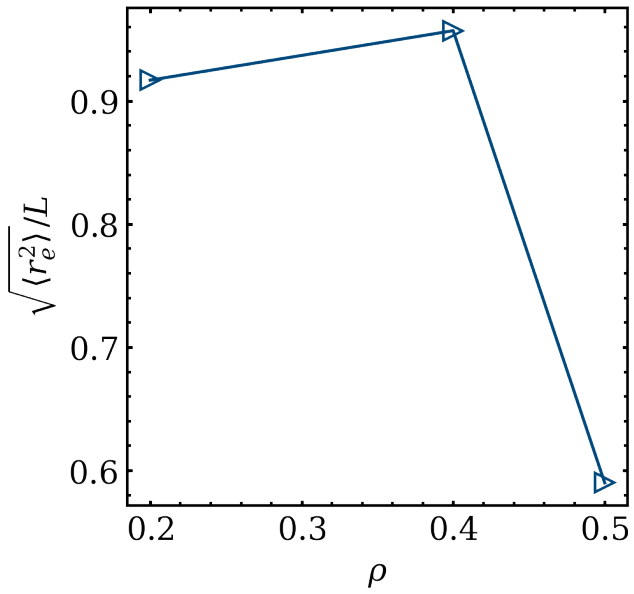

FIG. S6. The end-to-end distance, $\sqrt{\langle r_e^2 \rangle}/L$ for passive filaments ($Pe = 0$) at densities $\rho = 0.2, 0.4, 0.5$.

active polymers at high density [2] and passive systems [6].

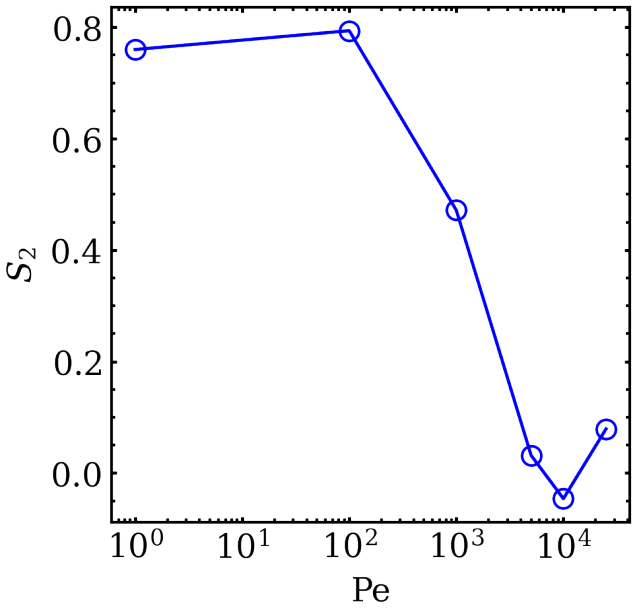

FIG. S7. Nematic order parameter S_2 defined in Eq. S6 as a function of Pe for a system at density $\rho = 0.4$.

LACK OF SYNCHRONIZATION BETWEEN DIFFERENT SPIRALS

As shown in the main text, spirals are present in the system at high Péclet numbers, and these spirals exhibit rotational motion. To investigate whether the spirals are synchronized, we compute the sign of the angular velocity ω. Figure S9 shows that the fraction of right-handed spirals ($\omega > 0$) is approximately 0.5, indicating an equal number of right-handed and left-handed spirals. Moreover, to verify whether neighboring spirals are synchronized, we compute the correlation function $\langle sign(\omega(r))\ sign(\omega(r + dr))\rangle$. Figure S10 shows this correlation function for a system in the

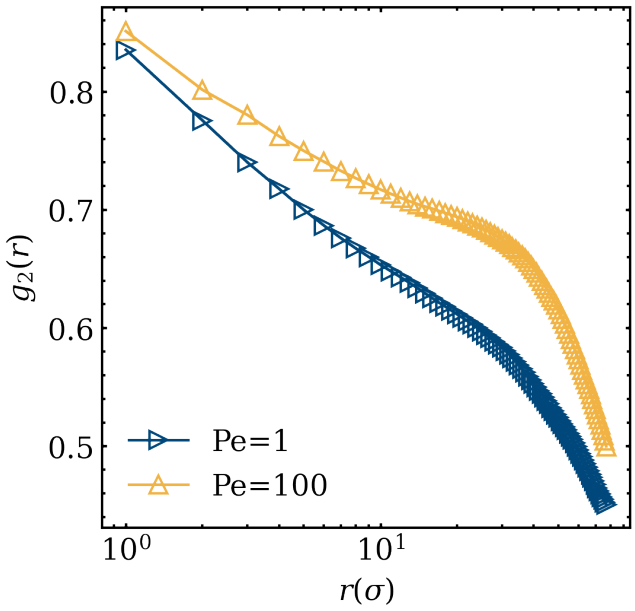

FIG. S8. Spatial correlation function $g_2(r)$ defined in Eq. S7 for the nematic order parameter as a function of the distance r for a system at density $\rho = 0.4$.

pure spiral phase ($Pe = 10^4$), demonstrating that neighboring spirals are not correlated, indicating the absence of synchronization between different spirals.

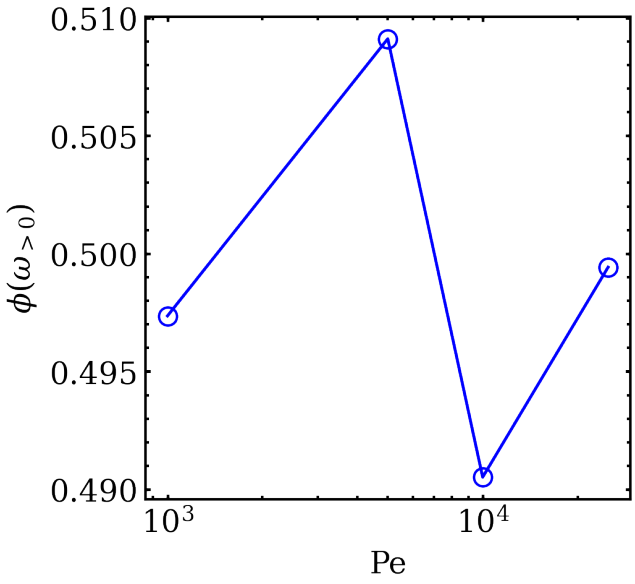

FIG. S9. Fraction of spirals with positive angular vecolity as a function of Pe for a system at density $\rho = 0.4$.

INERTIAL EFFECTS

Figure S11 shows the probability distribution of the turning number $P(\psi)$ for different damping coefficients γ for a single polymer. For small γ, the probability of finding open chains is small but non-zero (Fig. S11(a),(b)), while increasing γ, the probability of finding an open chain is zero. Additionally, the peaks of $P(\theta)$ shift with increasing γ, indicating that the spirals become progressively more compact as inertial effects become negligible.

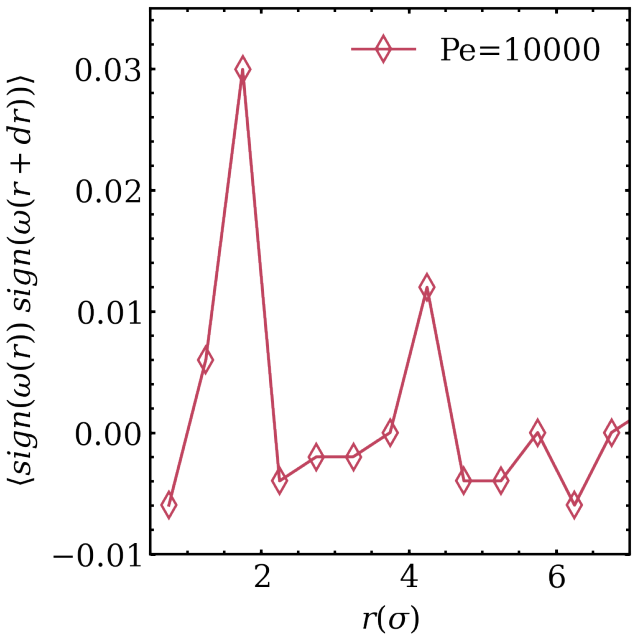

FIG. S10. Correlation function $\langle sign(\omega(r))\ sign(\omega(r+dr))\rangle$ as a function of the distance $r(\sigma)$ for a system at density $\rho = 0.4$.

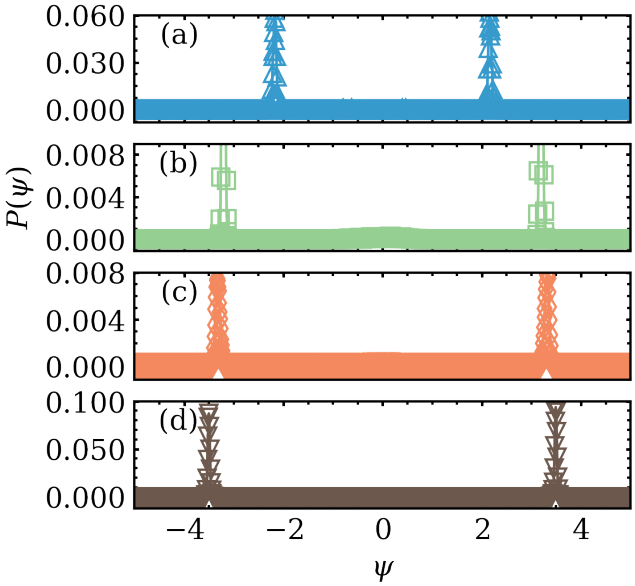

FIG. S11. Probability distribution of the turning number $P(\psi)$ for a single polymer. (a) The blue triangles represent $P(\psi)$ for $\gamma = 10^{-1}$. (b) The green squares correspond to $\gamma = 5 \times 10^{-1}$ (c) Orange diamonds represent $\gamma = 10^{0}$. (d) Brown upside-down triangles correspond to $\gamma = 10^{1}$.

To characterize the shape of the spiral as a function of the damping coefficient, we fit the spiral to Archimedean spirals. In Fig. S12, we show the fit for $\gamma = 10$ using the equation $r = a + b(c\theta + \theta_0)$, with the parameters: $a = 2.634$, $b = 0.109$, $c = -1.371$, and $\theta_0 = 11.522$. In Fig. S13, we present the fit for $\gamma = 1$ using the fitting parameters: $a = 2.687$, $b = 0.089$, $c = -1.7678$, and $\theta_0 = 14.945$. This figure illustrates how the fit to the Archimedean spiral starts to deteriorate as inertial effects become more significant, causing the spirals to become more logarithmic-like. In the video titled *gamma10.mp4*, where $\gamma = 10$ and $Pe = 2.5 \times 10^3$ for a system with $\rho = 0.4$, it's evident that spirals begin to form. This suggests that the transition to the pure spiral phase is shifted to higher Pe values. Additionally, the files *gamma001.mp4* and *gamma01.mp4* display videos for $Pe = 2.5 \times 10^3$ with $\gamma = 0.01$ and $\gamma = 0.1$, respectively. In these cases, characterized by small damping coefficients, the spiral phase is absent, and the filaments remain in a

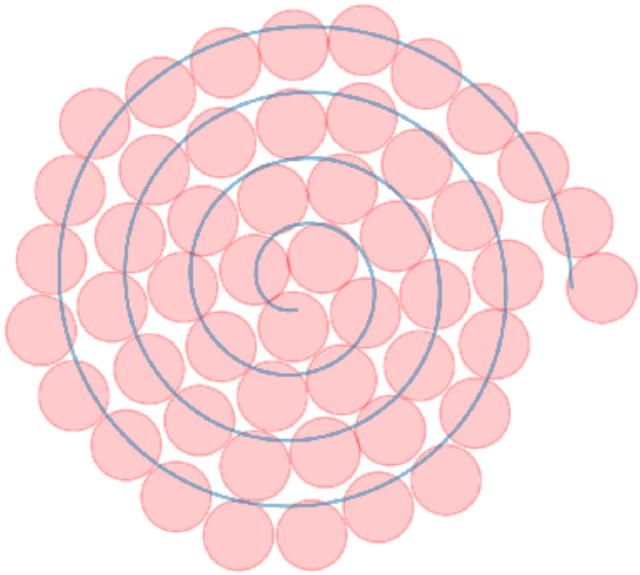

FIG. S12. Fit to Archimedean spirals for $\gamma = 10$ and $\rho = 0.4$. The fiting parameters are: $a = 2.634, b = 0.109, c = -1.371$, and $\theta_0 = 11.522$.

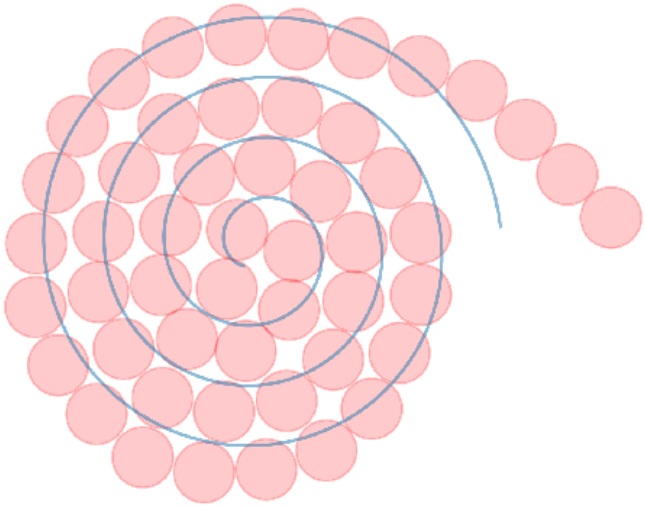

FIG. S13. Fit to Archimedean spirals for $\gamma = 1$ and $\rho = 0.4$. The fiting parameters are: $a = 2.687, b = 0.089, c = -1.7678$, and $\theta_0 = 14.945$.

highly compact open-chain state. The movies represent 50 snapshots, each of which is taken every $10^3\tau$ timesteps.

[1] H. Noguchi and G. Gompper, *Phys. Rev. E*, 2005, **72**, 011901.
[2] K. R. Prathyusha, S. Henkes and R. Sknepnek, *Physical Review E*, 2018, **97**, 022606.
[3] J. D. Weeks, D. Chandler and H. C. Andersen, *The Journal of chemical physics*, 1971, **54**, 5237–5247.
[4] A. Shee, N. Gupta, A. Chaudhuri and D. Chaudhuri, *Soft Matter*, 2021, **17**, 2120–2131.
[5] M. Doi, S. F. Edwards and S. F. Edwards, *The theory of polymer dynamics*, oxford university press, 1988, vol. 73.
[6] M. A. Bates and D. Frenkel, *The Journal of Chemical Physics*, 2000, **112**, 10034–10041.